A computational framework to simulate the endolymph flow due to vestibular rehabilitation maneuvers assessed from accelerometer data

Carla F. Santos[a], Jorge Belinha[b], Fernanda Gentil[c], Marco Parente[a], Bruno Areias[a] and Renato Natal Jorge[a]

[a]University of Porto, Faculty of Engineering, INEGI, Porto, Portugal; [b]Department of Mechanical Engineering, School of Engineering, Polytechnic of Porto, Portugal; [c]Clínica ORL - Dr. Eurico Almeida, Escola Superior de Saúde, Porto, Portugal

ABSTRACT

Vertiginous symptoms are one of the most common symptoms in the world, therefore investing in new ways and therapies to avoid the sense of insecurity during the vertigo episodes is of great interest. The classical maneuvers used during vestibular rehabilitation consist in moving the head in specific ways, but it is not fully understood why those steps solve the problem. To better understand this mechanism, a three-dimensional computational model of the semicircular ducts of the inner ear was built using the finite element method, with the simulation of the fluid flow being obtained using particle methods. To simulate the exact movements performed during rehabilitation, data from an accelerometer were used as input for the boundary conditions in the model. It is shown that the developed model responds to the input data as expected, and the results successfully show the fluid flow of the endolymph behaving coherently as a function of accelerometer data. Numerical results at specific time steps are compared with the corresponding head movement, and both particle velocity and position follow the pattern that would be expected, confirming that the model is working as expected. The vestibular model built is an important starting point to simulate the classical maneuvers of the vestibular rehabilitation allowing to understand what happens in the endolymph during the rehabilitation process, which ultimately may be used to improve the maneuvers and the quality of life of patients suffering from vertigo.

1. Introduction

Vertigo is a type of dizziness that normally occurs due to a dysfunction in the vestibular system, which is located in the inner ear. The patient has the perception of a spinning motion, a feeling of displacement of the environment relative to the individual or an intensive sensation of rotation inside the head (Taylor and Goodkin 2011). In these situations, it is important to avoid falls. Such symptoms are often associated with nausea and vomiting, and it can cause difficulties in standing or walking if it is related with central lesions (Karatas 2008). Other debilitating symptoms such as blurred vision and hearing loss may also occur (Strupp et al. 2011). Vertigo can be classified as either peripheral or central, depending on the location of the dysfunction in the vestibular pathway, and its most common cause is benign paroxysmal positional vertigo (BPPV) (Karatas 2008), although it can be caused by other factors (Wippold and Turski 2009).

1.1. Vestibular system

The vestibular system is the sensory system that provides the leading contribution about movement and sense of balance. As our movements consist of rotations and translations, the vestibular system comprises two connected main components; the three semicircular canals (SCCs), which are placed orthogonally to measure rotational movements, and the utricle and the saccule, which contain the otoliths to measure linear accelerations. Each SCC is comprised of a circular section of continuous fluid, connected with the ampulla and the vestibule (which contains the sensory epithelium).

The SCCs comprise the bony labyrinth, which enclose a membranous labyrinth with the same structure called semicircular ducts (SCD) containing the endolymph; between both labyrinths, another fluid called perilymph is present.

The hair cells of the ampulla rest on a tuft of blood vessels, nerve fibers, and supporting tissue called

cupula. The sensory-cells exhibit a constant discharge of neurotransmitters, which are modified by the direction of the cupula deflection, and this output signal has its origin in the velocity of head rotation. Thus, these cells placed in the cupula on the SCD, are known, in the engineering field, as "rate-sensor" (Herdman 2007).

1.2. Physical therapy evolution

The original treatment for vestibular disorders was developed in the 1950s and included a set of progressive exercises, called Cawthorne-Cooksey exercises (Cooksey 1946), designed to manage dizziness and improve balance following damage to the inner ear. More recently, techniques have been developed to address specific problems with gaze and postural instability, motion sensitivity, and vertigo in patients with a variety of vestibular disorders such as BPPV, Ménière's disease and others (Zhou and Cox 2004). Some studies (Deveze et al. 2014; Herdman 2013) have analyzed the use of advanced technologies, such as a "balance vest" providing patients with vibrotactile feedback to help them regain balance control. Other methodologies include computerized techniques to help restore steady vision during head movements (gaze stability) and to document improvements in the ability to focus on tasks in the presence of distractions (perceptual and motor inhibition). A device similar to a mirrored "disco ball" has been used to provide optokinetic stimulation for patients with vestibular disorders (Pavlou 2010). Another study (Cox & Jeffery 2010) shows that gaze stability exercises can reduce the risk of falling in older adults with vestibular disorders. Further works (Honaker et al. 2012) show the effectiveness of vestibular rehabilitation on vestibular-visual-cognitive function following blast-induced head trauma sustained by soldiers in war, while in another study (Alsalaheen et al. 2010) an improvement in dizziness, walking and balance was reported after a customized vestibular physical therapy program in children and adults with concussion was developed. All these studies are crucial to document the effectiveness of specific rehabilitation techniques for specific groups of patients with different vestibular dysfunctions.

1.3. Vestibular Rehabilitation

Vestibular rehabilitation is becoming an interesting treatment option for a patient with dizziness and balance problems, because such therapy can improve symptoms, functioning, and compliance (Boyer et al. 2008). The vestibular rehabilitation exercises stimulate the brain to use visual clues and proprioceptive alternatives to maintain balance and gait, and there is evidence that it improves nystagmus, control postural dizziness and all other vertigo symptoms, making it the definitive treatment for most patients (Swartz & Longwell 2005). Specific methods include maneuvres to repositioning otoliths, adaptation or substitution exercises that can be vestibular-ocular, vestibular-cervical, or vestibular-spinal, spatial-orientation. Non-specific methods consist generally in rehabilitating overall endurance and strengthening specific muscle groups to sustain posture or balance. The fact that good results can be obtained without drug side effects and that the treatment is both convenient and targeted leads to a gain in confidence by the patient in carrying out its daily activities (Herdman 2013). The first empirical vestibular rehabilitation programs were developed for subjects presenting brain injuries, and later on, the hypothesis of canalithiasis (when the otoconia are loose within the fluid pathways of the inner ear) in the SCD was validated by the success of dislodging maneuvers (Boyer et al. 2008). Physical therapists play a central role in vestibular rehabilitation, not only as care providers but also in helping advance new research in the field. The next wave of vestibular rehabilitation approaches could include virtual reality feedback and training, vestibular implants, and even stem cell techniques (Pavlou 2010; Herdman 2013). With the ultimate goal of improving the quality of life of persons with vestibular disorders, it is important to study the problem from a multi-disciplinary point of view, such that physical therapists, engineers, and physicians all contribute to better understand how the vestibular system works to improve rehabilitation techniques.

1.4. Motivation

Although various treatments exist, none can be confidently labeled as the best option because not enough scientific evidence exists, both due to the questionable efficacy of controlled studies and also the difficulty in obtaining data from randomized clinical trials (Boyer et al. 2008). As stated by Herdman (Herdman & Clendaniel 2014), the phenomena that occur during treatment should be correctly identified in order to develop better rehabilitation procedures, and computational models can greatly help study the vestibular system. The present study aims to computationally

model the exact movements performed in that procedure.
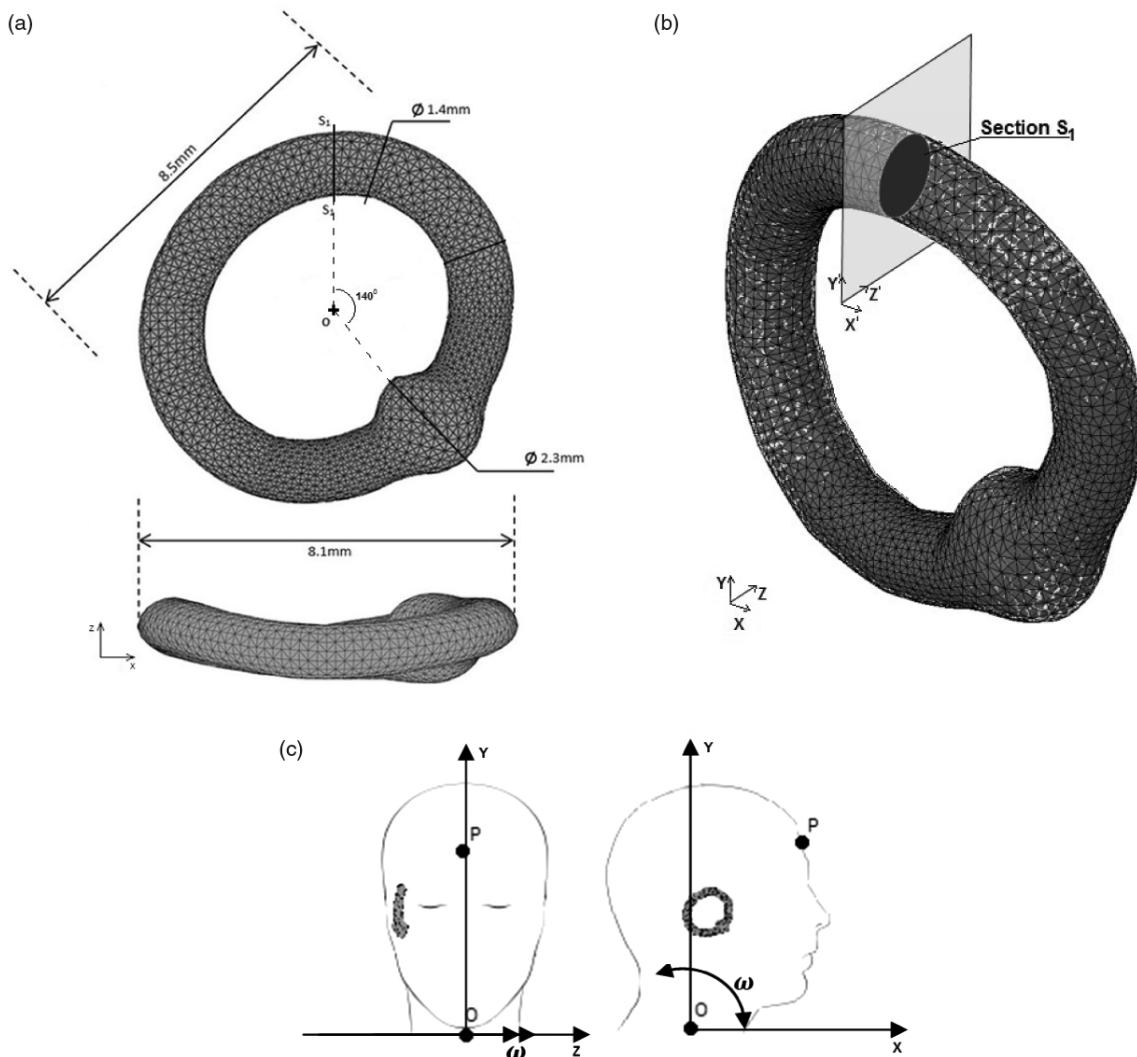
2. Methods

Studying the movements made during the vestibular maneuvers is the most important step in the rehabilitation process. To this end, such movements were performed by a qualified physical therapist (audiology expert) on a patient and were registered by an accelerometer, which is used to measure acceleration (and consequently velocity and displacement by integration).

2.1. Accelerometer data collection

The accelerometer used in the present work (available in Porto Biomechanics Laboratory) is a BIOPAC© device. The accelerometer was placed in a specific position in the forehead of the patient (point P shown in Figure 1(a)) while the audiologist performed the maneuvers, and data were collected using a sampling rate of 200 Hz. The accelerometer location was chosen
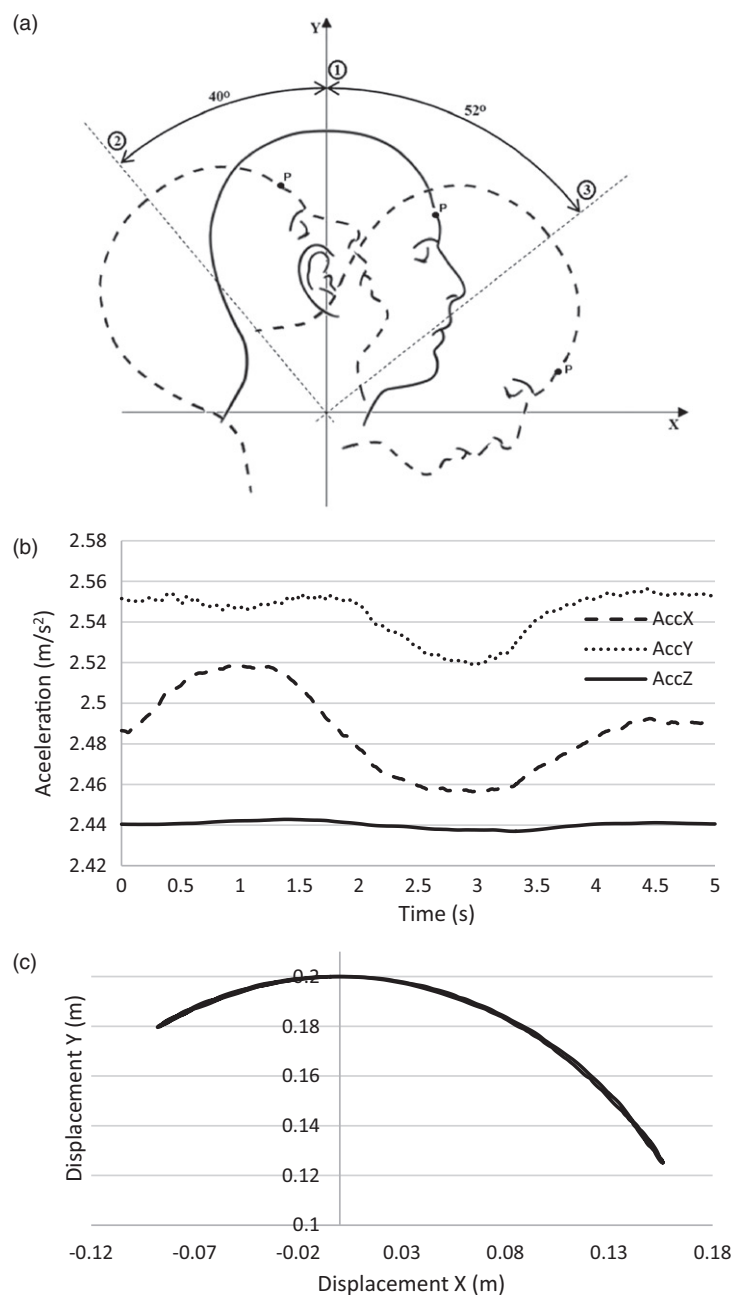
Figure 1. (a) Movement performed with the accelerometer, flexion-extension. (b) Acceleration for the movement of the neck. (c) Displacement in the sagittal plane.

Figure 2. Model of one SCC built in finite element method, (a) dimensions of the model, (b) particles inside the canal and Section S_1, and (c) Scheme of the position of the model in the human body and the accelerometer.

to capture the movement in the sagittal plane, which is the main plane of the flexion-extension movement.

To test the proposed method, a movement of flexion-extension of the neck was measured, starting by move the head backward and followed by a movement forward until the maximum possible angle (Figure 1(a)). The data obtained from the accelerometer was in volts, which were then converted to g-units and then to the SI units (m/s^2) in the three principal axes. Figure 1(b,c) shows the displacement obtained from the accelerometer data (since that the movements performed during the flexion-extension of the neck happened mainly in the sagittal plane as shown in Figure 1(b)). The data were also normalized to zero mean. This movement was the one related with the anterior canal of the vestibular system, which is the most affected by vertigo symptoms in the case of dehiscence syndrome.

Since this is a preliminary study, a simple subset of the full Semont maneuver (Califano et al. 2014) was selected to allows the validation of the proposed numerical approach. The displacement shown in Figure 1(c), obtained by double integration and posterior trigonometric relations due to the angular movement, was applied to the finite element model of the SCD described in the next section in order to simulate the real flexion-extension movement.

2.2. Finite element model characterization

The software used to build the model of the vestibular system with finite elements is ABAQUS® (Hibbit & Karlsson 2004). This software is one of the most well-known and robust computational frameworks developed for finite element analysis, mainly used for solid
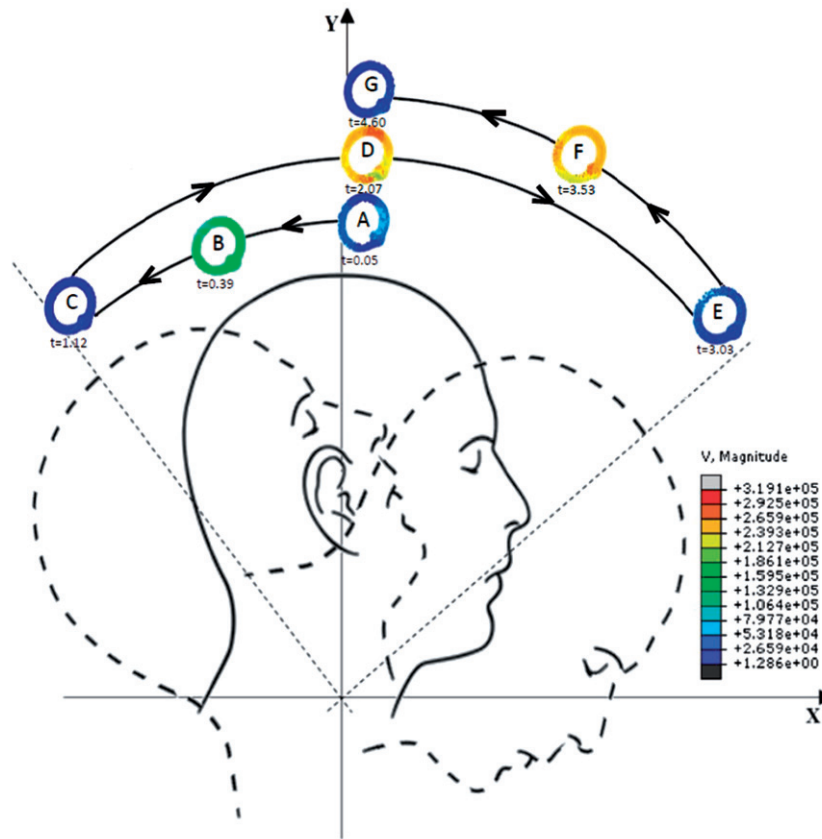
Figure 3. Velocity(m/s) of the fluid along the movement.

models but also successfully used to study biological models (Gentil et al. 2011).

The developed 3D model was composed of two main parts: a shell ring that represents one SCD, as shown in Figure 2(a), and inside the ring are particles that represent the endolymph fluid. The model represents the vestibular membrane of the SCD and it is defined as a rigid body, which is a model simplification in order to reduce the computational cost and simulation complexity. The kind of elements used for the shell are linear 4-node shell (S4R). Section S_1 (Figure 2(b)) is coincident with the section of the YZ plane where the fluid will be analyzed. The properties of the endolymph used in the model follow those described in the literature (Wu et al. 2011): a density of 1.0×10^{-3} kg/m^3 and a viscosity of 4.8×10^{-3} Pa.s.

The boundary conditions imposed in the model include the general contact between the membrane and the fluid, the gravitational force and finally the angular movement. The model shown in the Figure 2(b) illustrates the SCD filled with fluid with the section analyzed. The dots inside the duct represent the discrete particles related to the endolymph. The simulation of the particles movement is performed considering the

Smoothed Particle Hydrodynamics (SPH) method, which is a meshless method, widely used in bio-fluid simulations (Liu and Liu 2003; Ye et al. 2016). The dimensions of the model were obtained from a CT-scan of the SCC, with more detailed information about that procedure available in a previous work (Santos et al. 2017). An updated survey concerning geometric models and SPH applications to biomechanics (Santos et al. 2017), shows the reduced number of research works simulating this important pathology. In the scheme represented in Figure 2(c), point O represents the instantaneous center of rotation, which is in accordance with one of the degrees of freedom of the neck in the yOz plane, allowing the flexion-extension movement. Therefore, in the represented movement, only rotations around the Oz axis are allowed.

Notice that Figure 2(c) does not represent a real scale canal, as the dimensions are enlarged for easier understanding. As already mentioned, from the accelerometer it is possible to obtain the linear acceleration. Thus, using the following kinematic equation, it is possible to obtain the displacement field at any given time in a point belonging to the head represented in Figure 2(c),
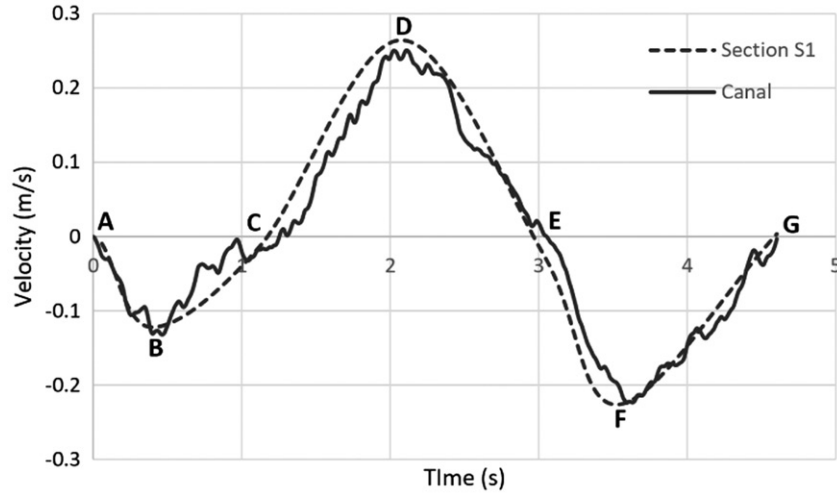
Figure 4. Smoothed average x-velocity component in section S_1 and the canal.

$$\vec{u}(t) = \begin{cases} 0 \\ R\sin(\omega(t)) \\ R\cos(\omega(t)) \end{cases} \quad (1)$$

Being R the Euclidian distance between O & an interest point in the head. With the displacement field fully defined, in Cartesian coordinates, it is possible to define the velocity,

$$\frac{d\vec{u}(t)}{dt} = \vec{v}(t) = \begin{cases} 0 \\ R\dfrac{d\omega(t)}{dt}\cos(\omega(t)) \\ -R\dfrac{d\omega(t)}{dt}\sin(\omega(t)) \end{cases} \quad (2)$$

and then the acceleration field,

$$\frac{d\vec{v}(t)}{dt} = \vec{a}(t) = \begin{cases} 0 \\ R\dfrac{d^2\omega(t)}{dt^2}\cos(\omega(t)) - R\left(\dfrac{d\omega(t)}{dt}\right)^2\sin(\omega(t)) \\ -R\dfrac{d^2\omega(t)}{dt^2}\sin(\omega(t)) - R\left(\dfrac{d\omega(t)}{dt}\right)^2\cos(\omega(t)) \end{cases}$$

$$(3)$$

Knowing the exact position of point P & point O, it is possible to obtain R. In this work, $R = 0.2\,m$ was used, since it represents an approximated measured distance from the neck to the inner ear. Then, matching Equation (3) to the acceleration coming from the accelerometer, it was possible to obtain the instantaneous angular velocity $\omega(t)$. Knowing the approximate location of the vestibular system, point Q, it was possible to determine a new $R = \|\overline{OQ}\|$, which is inserted in Equation (1) to obtain the displacement field of the vestibular system in Cartesian coordinates.

After the simulation performed the results were obtained & analyzed.

3. Results

Simulations were carried out using the parameters defined in the previous section, & the results regarding fluid velocity along the duct are shown in Figure 3, where various frames ranging from A to G cover the totality of the experimentally measured head movement.

The A, D & G frames correspond to location 1 in Figure 1(a) but to different instants of the simulation, while frames C & E correspond to the instants when there is a change in the direction of movement, visible due to the lower velocities, & refer to position 2 & 3 in Figure 1(a) respectively. Finally, frames B, D, & F are the ones with higher velocity, coinciding with the midway moments between each change in direction. After this preliminary analysis, one section of the duct (S_1 showed in Figure 2(b)) was analyzed. Figure 4 shows the averaged x-velocity component of the fluid particles in section S_1 along the simulation, compared with the x-velocity component of the duct. The letters correspond to the same moments as in Figure 3.

A representation of the fluid path inside the duct is illustrated in Figure 5, which shows five different paths with different initial locations (point I), to simulate the start of the simulation at different quadrants of the duct apart from the locations anterior & posterior to the cupula. Figure 5 shows the real movement of the fluid inside the duct. Thus, the path of five different fluid particles was shown inside the duct. At the beginning of the analysis, five particles (representing distinct finite volumes of fluid, at distinct spatial positions) were selected: particle **a**, **b**, **c**, **d**, & **e**, respectively represented in Figures 5(a–e). The five different locations were selected in relevant positions, such as posterior & anterior to the cupula (particles **a** & **b** respectively), in the opposite position to the cupula (particle **c**) & in the halfway distance between the cupula & particle **c**
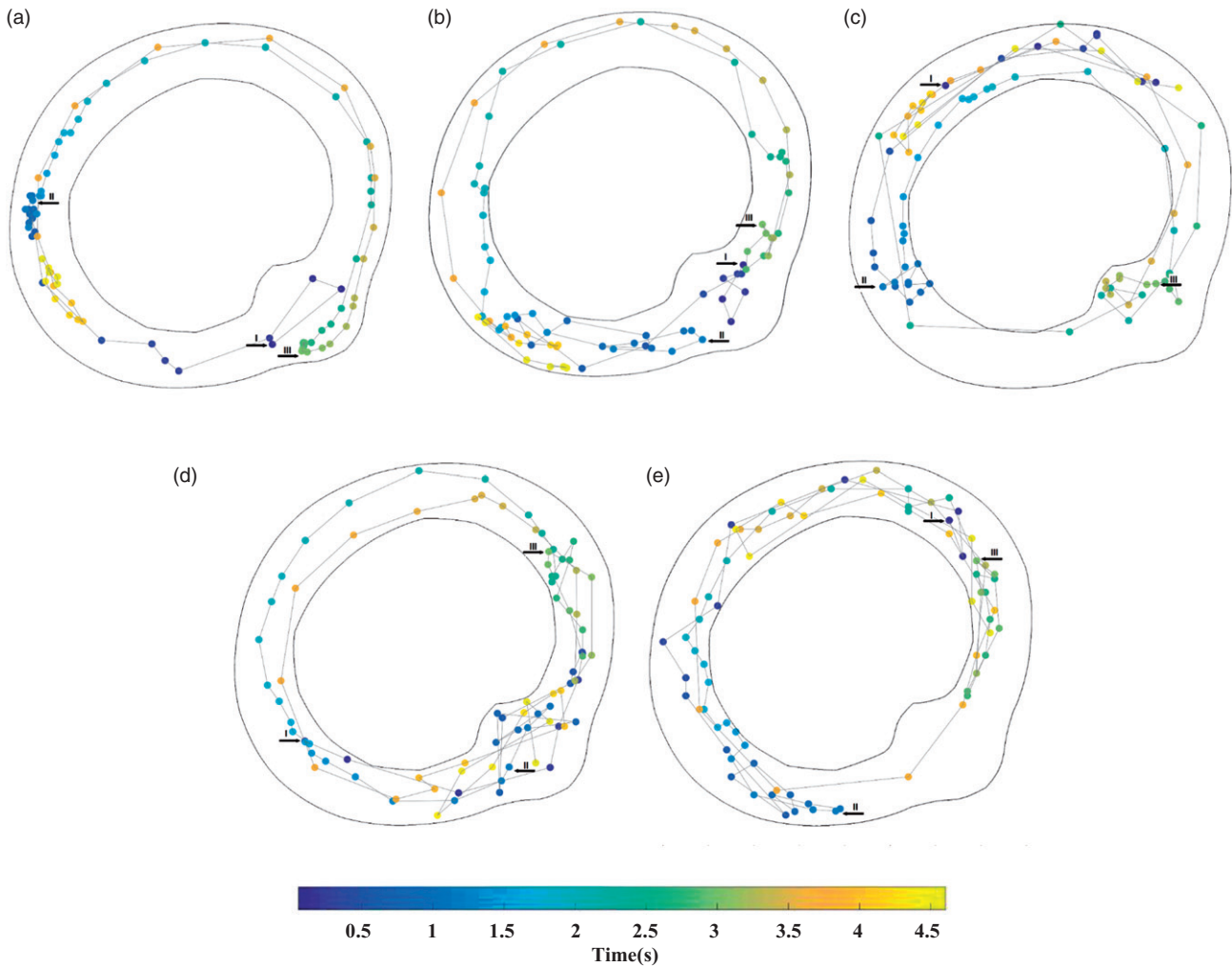
Figure 5. Particle path along the simulation, in seconds, starting in five different locations: (a) posterior to the cupula, (b) anterior to the cupula, (c) opposite position to the cupula, (d) halfway distance between the cupula and particle c in left side, and (e) halfway distance between the cupula and particle c in right side.

(particles **d** & **e**, respectively). Such analysis intends to understand the influence of the initial position of the particle in its trajectory.

Therefore, the motion of these particles was tracked. Allowing to capture a global position with respect to time. In the figure, it is possible to see the trajectory of the particle along time. Furthermore, to enhance the comprehension of the trajectory, in Figure 5, a color bar is included indicating the time step of the analysis (in seconds). Thus, the blue color represents the particle at the initial time & the yellow color represents the position of the same particle at the final time.

Notice that the particle alters its movement direction (see point II & point III) at the same instant as the head movement change (frames C & E in Figure 3).

4. Discussion

The representation of fluid velocity along the SCD, shown in Figure 3, seems to follow what would be

expected: the beginning & end of the simulation (frames A & G, respectively) present velocities very close to zero, as do the points of the simulation where change of direction occurs (frames C & E). This is expected because near the beginning of the simulation the fluid is still gaining traction (after being completely still at $t = 0$ s), while in both changes of direction (frames C & E) the value is naturally low due to the fact that the head is stopped in a specific instant (therefore only the residual fluid velocity from the immediately previous instant affects the distribution of velocities), & the same reason justifies the velocity profile of the end frame G (the head stops moving at that point). The remaining frames (B, D & F) all present considerable velocity values, which is in accordance with the fact that such frames refer to instances where the head is moving in a certain direction, which induces movement in the fluid. Regarding the relative magnitude of the fluid velocity for those frames, frame B presents the lowest values due to it

occurring shortly after the start of the simulation & also that the angle between frames A & C is 40° (Figure 1(a)), while frame D corresponds to a time step specifically in the middle of C to E which spans 92° of movement, thus a higher magnitude of the movement is expected as the fluid has more time to reach a higher velocity. Finally, frame F is in the middle of a 52° movement, which explains why the velocity magnitude is higher than frame B but slightly lower than frame D.

The range of movement obtained in the sagittal plane are in agreement with the average angle for the flexion-extension of the neck found in the literature (Dunleavy and Goldberg 2013). The amplitude of the neck movement is higher in the anterior part of the body like the results shows. The 0.20 m used as reference in Figure 1(c) is the average distance from the neck to the inner ear.

Figure 4, which shows the average fluid velocity across section S_1 as a function of simulation time, follows a similar trend: instants C and E, where the velocity is zero, correspondi to the instants around seconds 1 and 3 in Figure 1(b), where the x-component of the acceleration changes its direction. Such change in direction corresponds to the derivative being zero, which confirms the results presented in Figure 4 and the velocity magnitudes in Figure 3. Comparing both curves in Figure 4, both velocities present similar results, indicating the reliable behavior of the model towards the imposed displacement, which is what was expected. The average velocity of all particles in section S_1 is also an indicator of result reliability, as higher velocities correspond, as expected, to the longer part of the movement without direction changes, between point 2 and 3 (see Figure 1(a)).

As for Figure 5, it is visible that the starting point of the analysis influences the results, which is expected due to the varying geometry of the duct, which affects the dynamics of the fluid in different ways and is what happens in the real situation due to this model geometry being similar to the geometry of the inner ear. The pathway between point I and II is the shortest, as expected, compared with the one between point II and III. This output, obtained in Figure 5, reveals the possibility to track/analyse any particle fluid or otoconia path inside the SCD during the simulation.

Comparing the results obtained with the chosen particles it is possible to observe that particles **a** and **b** (posterior and anterior to the cupula) are the ones with the best-defined path along the duct. This behavior could be a helpful guide in the common BPPV cases where the otoconia rest near the cupula. Also,

the distance between two color points allows us to conclude if the analyzed particle is slower or faster in each specific part. Particles **c** and **e**, which start their path in the superior part of the duct, appear to show slower movements, as the points looks closer between each other. All the selected particles showed a final position (the yellowest spot) at a similar distance from the initial position in the five paths.

These results show the effectiveness of the model and prove that it is possible to infer about the inner movement of the endolymph and, consequently, the movement of otoconia. Nevertheless, the authors would like to clarify that the model has some limitations that should be considered, as the structure of the ducts and the canals. In future works, the model of the vestibular system should be enhanced to include the vestibules and the crus commune in order to obtain simulation outcomes closer to the anatomical system. Additionally, despite the limitations, the current model showed similar results with other authors (Santos et al. 2017).

Since all the maneuvers performed in the vestibular rehabilitation are based in angular movements, it appears that the used method, based in trigonometric relationships, is a valid numerical technique to deduce the displacement of the head, allowing for successful simulations based in the accelerometer data.

5. Conclusion

The main aim of this work is to improve the knowledge on the vestibular rehabilitation process. Since the vestibular rehabilitation performed nowadays consist in a set of movements which lack accuracy and consistent reproducibility, the method presented in this paper intends to be a step to improve this procedure. An overall analysis of the results shows that such main aim was achieved. Data obtained using an accelerometer from a patient treated by a qualified physical therapist was combined with a finite element model to simulate the flexion-extension movement of the SCC, and the results allow us to validate this method as a starting point of the rehabilitation maneuvers simulation, as the fluid velocity distribution as a function of analysis time is coherent and follows the head movement. This work is an important first step both because it validates the model and also because it is focused on the less studied canal associated with BPPV, which opens the way for further studies into the diseases occurring in this canal, as emphasized by Herdman (Herdman 2013).

The study of vestibular rehabilitation is also very important as it is a treatment for vestibular disorders which does not administers drugs (Rosengren et al. 2010), making it a natural alternative free of pharmaceuticals. As for future work, this model should be tested using the same method under different conditions – such as the three more common maneuvers used in the vestibular rehabilitation.

In conclusion, the use of computational simulation is an exceptional opportunity to create realistic simulations in biomedicine, as proved in this research work where the movements involved in vestibular rehabilitation was numerically reproduced.

References

Alsalaheen BA, Mucha A, Morris LO, Whitney SL, Furman JM, Camiolo-Reddy CE, Collins MW, Lovell MR, Sparto PJ. 2010. Vestibular rehabilitation for dizziness and balance disorders after concussion. J Neurol Phys Ther. 34(2):87–93.

Boyer FC, Percebois-Macadré L, Regrain E, Lévêque M, Taïar R, Seidermann L, Belassian G, Chays A. 2008. Vestibular rehabilitation therapy. Neurophysiol Clin. 38(6):479–487.

Califano L, Salafia F, Mazzone S, Melillo MG, Califano M. 2014. Anterior canal BPPV and apogeotropic posterior canal BPPV: two rare forms of vertical canalolithiasis. Acta Otorhinolaryngol Ital. 34(3):189–197.

Cooksey FS. 1946. Rehabilitation in Vestibular Injuries. Proc R Soc Med. 39(5):273–278.

Cox PG and Jeffery N. 2010. Semicircular canals and agility: the influence of size and shape measures. J Anat. 216(1):37–47.

Deveze A, Bernard-Demanze L, Xavier F, Lavieille J-P, Elziere M. 2014. Vestibular compensation and vestibular rehabilitation. Current concepts and new trends. Neurophysiol Clin. 44(1):49–57.

Dunleavy K and Goldberg A. 2013. Comparison of cervical range of motion in two seated postural conditions in adults 50 or older with cervical pain. J Man Manip Ther. 21(1):33–39.

Gentil F, Parente M, Martins P, Garbe C, Jorge RN, Ferreira A, Tavares JM. 2011. The influence of the mechanical behaviour of the middle ear ligaments: a finite element analysis. Proc Inst Mech Eng H. 225(1):68–76.

Herdman S. 2007. Vestibular rehabilitation. F.A. Davis, Philadelphia.

Herdman SJ, Clendaniel R. 2014. Vestibular Rehabilitation (Contemporary Perspectives in Rehabilitation) 4th Edition. F.A. Davis, Philadelphia.

Herdman SJ. 2013. Vestibular rehabilitation. Curr Opin Neurol. 26(1):96–101.

Hibbit SPD, Karlsson B. 2004. Software License Agreement for Academic Institutes, ABAQUS: Theory Manual", Providence, USA.

Honaker JA, Tomasek R, Bean K, Logan B. 2012. Impact of visual disorders on vestibular and balance rehabilitation therapy outcomes in soldiers with blast injury. Int Tinnitus J. 17(2):124–133.

Karatas M. 2008. Central vertigo and dizziness. Neurologist. 14(6):355–364.

Liu GR, Liu MB. 2003. Smoothed Particle Hydrodynamics. WORLD SCIENTIFIC, Singapore.

Pavlou M. 2010. The use of optokinetic stimulation in vestibular rehabilitation. J Neurol Phys Ther. 34(2):105–110.

Rosengren SM, Welgampola MS, Colebatch JG. 2010. Vestibular evoked myogenic potentials: past, present and future. Clin Neurophysiol. 121(5):636–651.

Santos CF, Belinha J, Gentil F, Parente M, Jorge RN. 2017. An alternative 3D numerical method to study the biomechanical behaviour of the human inner ear semicircular canal. Acta Bioeng Biomech. 19(1):3–15.

Strupp M, Thurtell MJ, Shaikh AG, Brandt T, Zee DS, Leigh RJ. 2011. Pharmacotherapy of vestibular and ocular motor disorders, including nystagmus. J Neurol. 258(7):1207–1222.

Swartz R, Longwell P. 2005. Treatment of vertigo. Am Fam Physician. 71(6):1115–1122.

Taylor J, Goodkin HP. 2011. Dizziness and vertigo in the adolescent. Otolaryngol. Clin North Am. 44(2):309–321.

Wippold FJ, Turski PA. 2009. Vertigo and Hearing Loss AJNR. Am J Neuroradiol. 30(8):1623–1625.

Wu C, Hua C, Yang L, Dai P, Zhang T, Wang K. 2011. Dynamic analysis of fluid-structure interaction of endolymph and cupula in the lateral semicircular canal of inner ear. J Hydrodyn Ser B, 23(6):777–783.

Ye T, Phan-Thien N, Lim CT. 2016. Particle-based simulations of red blood cells-A review. J Biomech. 49(11):2255–2266.

Zhou G and Cox LC. 2004. Vestibular evoked myogenic potentials: history and overview. Am J Audiol. 13(2):135–143.